Atmospheric Environment 189 (2018) 145–152

Contents lists available at ScienceDirect

Atmospheric Environment

journal homepage: www.elsevier.com/locate/atmosenv

Aerosol optical absorption coefficients at a rural site in Northwest China: The great contribution of dust particles

Xueqin Wu[a], Jun Liu[a], Yunfei Wu[b,*], Xin Wang[a,**], Xiaowei Yu[c], Jinsen Shi[a], Jianrong Bi[a], Zhongwei Huang[a], Tian Zhou[a], Renjian Zhang[b]

[a] Key Laboratory for Semi-Arid Climate Change of the Ministry of Education, College of Atmospheric Sciences, Lanzhou University, Lanzhou, 730000, China
[b] CAS Key Laboratory of Regional Climate-Environment for Temperate East Asia (RCE-TEA), Institute of Atmospheric Physics, Chinese Academy of Sciences, Beijing, 100029, China
[c] South China Institute of Environmental Sciences, Ministry of Environmental Protection, Guangzhou, 510655, China

ARTICLE INFO

Keywords:
Dust aerosol
Black carbon
Dust storm
Mass absorption efficiency

ABSTRACT

An intensive measurement campaign was conducted at a rural site in Northwest China to investigate aerosol optical absorption properties, using the ground-based mobile facility of the Semi-Arid Climate and Environment Observatory of Lanzhou University (SACOL). The average mass concentration of $PM_{2.5}$ was 103 ± 4 μg m^{-3} during the 20-day campaign in April 2014. Black carbon (BC) only accounted for ~0.4% of the $PM_{2.5}$ on average, with the mean concentration of 443 ± 12 ng m^{-3} measured using a single particle soot photometer (SP2). The aerosol absorption coefficient (σ_{ap}) was 5.69 ± 0.01 Mm^{-1} on average, recorded by a multi-angle absorption photometer (MAAP) at the wavelength of 637 nm. It showed a linear relationship with BC mass concentration during non-dust periods, especially at their diurnal peaks of 07:00–09:00 a.m. (local standard time), deriving a bulk mass absorption efficiency (MAE) for BC of 8.5 ± 1.1 m^2 g^{-1}. The σ_{ap} increased sharply during the dust storm, while the BC remained at a lower concentration than other moments, implying that the dust particles had a considerable contribution to light absorption. On average, dust particles accounted for 26.7% of the aerosol absorption and increased to 71.6% during the dust storm. The MAE of dust was calculated to be 0.014 ± 0.00028 m^2 g^{-1}, which was comparable to that measured in the downwind regions in East Asia. Based on the Mie theory for spherical particles, the refractive index (m) of natural mineral dust particles was estimated to be 1.50–0.0007i in Northwest China.

1. Introduction

Certain aerosol components can enhance solar light absorption in the atmosphere, resulting in a warming effect on the regional and global climates (Ramanathan and Carmichael, 2008; Uno et al., 2009). Black carbon (BC) is a strongly light-absorbing aerosol of the incoming solar radiation, emitted from incomplete combustion of fossil fuels or biomass (Novakov et al., 2003). Although BC has a short atmospheric lifetime of a few weeks at most, the mixing of BC with other aerosol components can lead to varying degrees of enhancement in the BC absorption (Ramanathan and Carmichael, 2008). In addition, the deposition of BC aerosol can reduce the albedo of surfaces such as snow and ice. BC has a strong absorption centered in the visible and parts of the infrared spectrum with a small variation range of light absorption (Bergstrom et al., 2007). Generally, its absorption shows an inverse relation with the incident light wavelength (λ). Brown carbon (BrC) and mineral dust are considered as the other important contributors to aerosol absorption in the atmosphere. However, they strongly absorb solar radiation in near ultraviolet (UV) and blue light region, exhibiting a stronger wavelength dependence than BC (Kirchstetter et al., 2004; Andreae and Gelencser, 2006; Bond and Bergstrom, 2006; Yang et al., 2009). Alexander et al. (2008) pointed that massive BrC aerosols exist in East Asia (e.g., Beijing), derived from low-temperature biomass and biofuel burnings as well as multiphase processes (Lukács et al., 2007). Nevertheless, mineral dust dominates the aerosol mass over some regions in China and the mineral dust emitted in the desert regions of northwestern China contains 600 Tg, which may reach the half of that on the global scale (Husar et al., 2001; Boucher et al., 2013). Dust aerosols can travel eastward over long distances in the lower troposphere and then trigger more dust events (Uno et al., 2009; Pu et al., 2015; Wang et al., 2015b). They also absorb effectively in the infrared region, acting like a greenhouse gas with trapping outgoing radiative

* Corresponding author.
** Corresponding author.
E-mail addresses: wuyf@mail.iap.ac.cn (Y. Wu), wxin@lzu.edu.cn (X. Wang).

https://doi.org/10.1016/j.atmosenv.2018.07.002
Received 27 April 2018; Received in revised form 24 June 2018; Accepted 1 July 2018
Available online 02 July 2018
1352-2310/

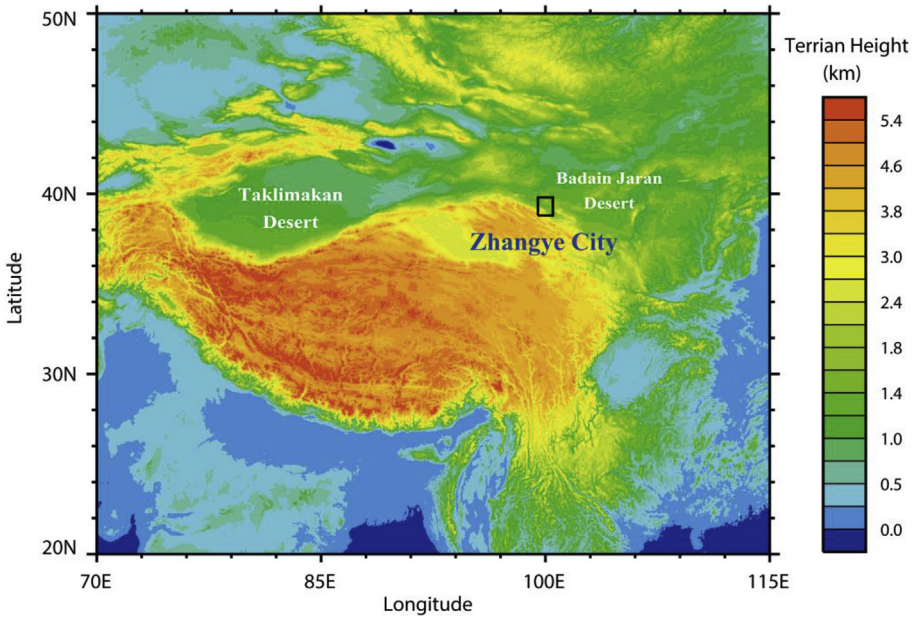

Fig. 1. The sampling site of Linze farm in Zhangye city and surrounding dust source areas.

(Andreae, 1996). As the predominant absorptive components of aerosols (Niu and Zhang, 2010), all three play an active role in heating the aerosol layer and promoting the increase in air temperature. Due to the high temporal and spatial variability in aerosol optical and physical properties, including refractive indices, size parameters and mixing states, large uncertainties exist in the assessment of the radiative effect induced by aerosol absorption (Boucher et al., 2013).

The most important sources for East Asian mineral dust has been identified as the northwestern regions of China, with the Taklimakan Desert, Gobi Desert and Badain Jaran Desert as their centers (Zhang et al., 2003; Huang et al., 2006; Wang et al., 2008, 2018a). Compared to background aerosol, the heating effect in the atmosphere of dust aerosols during dust event periods is more significant, and the contribution to averaged shortwave radiative forcing by the dust effect in the atmosphere was $\sim 28.21\ \mathrm{W\,m^{-2}}$ in Lanzhou (Liu et al., 2011). Furthermore, dust has a warming influence at the top of atmosphere when it exists under a cloud, reducing the cloud cooling effect (Su et al., 2008; Huang et al., 2014). Some evidence suggests that dust can produce the longwave warming effect at the surface during the night, because of their high absorption within the infrared spectrum (Choobari et al., 2014). Large size and non-spherical morphology make dust particles have greater optical depth and be better absorbers. Although the absorption efficiency of dust aerosols is generally smaller than that of BC aerosols, its contribution to the bulk absorption cannot be ignored during heavy dust pollution episodes due to the substantial atmospheric mass loading of dust particles. The magnitude of dust absorption and refractive indices differ according to the particle size distribution, composition and shape (Sokolik and Toon, 1999), which vary and depend on the source regions of emission (e.g., African and Asian dust), on the surface wind velocity (Jeong, 2008; Laurent et al., 2008), and especially on the physical and chemical aging degree during transport (Sullivan et al., 2007). Anthropogenic aerosol components such as BC, sulfates and nitrates can attach to the dust surfaces, eventually modifying the dust absorption properties (Falkovich, 2004).

In previous studies, different regions and emission sources exhibited disparate values of mass absorption efficiency (MAE) for BC, which vary to a large extent ($3.4–16.8\ \mathrm{m^2\,g^{-1}}$). It is also suggested that enhancement of MAE by the mixing of BC with non-refractory particulate matter largely depends upon the coating chemicals and mass (Lan et al., 2013). A much larger MAE of BC aerosol was observed at urban sites ($11.3 \pm 2.2\ \mathrm{m^2\,g^{-1}}$) than rural sites in India ($6.1 \pm 2.0\ \mathrm{m^2\,g^{-1}}$), indicating a high fluctuation in it (Ram and Sarin, 2009). Numerous discussions and analysis were addressed about absorption coefficient and relevant variation characteristics of BC in northwestern China. For example, Cao et al. (2014) mentioned that aerosol absorption coefficient had apparent daily variation almost the same as BC mass concentration on normal weather conditions. However, there was insufficient information on BC mass absorption efficiency in this area, which is widely used as a quantitative parameter for estimation in BC absorption. Unlike in the other regions, abundant dust particles of the northwest can act as an outer covering on the BC as well, further strengthening the BC absorptive capacity (Oshima et al., 2009). The supplementation of MAE data is of great importance to the accurate evaluation and improvement of environmental quality. To understand the radiation characteristics of atmospheric aerosols more comprehensively and more deeply, we carried out a surface observation in spring (frequent occurrences of dust events) and discuss the absorption properties of dust and BC aerosols in the northwestern desert regions in this study.

2. Methodology

2.1. Site description and meteorological conditions

The field experiment was conducted on farmland in Zhangye city, Gansu Province in northwest China (39.04°N, 100.12°E); this area is situated in the middle of the Hexi Corridor (1578 m above sea level). A ground-based mobile facility of the Semi-Arid Climate and Environment Observatory of Lanzhou University (SACOL) was used for this campaign from 9 to 28 April 2014. The north and south sides of the Hexi Corridor are both flanked by mountains, leading to the formation of a long and narrow area which runs approximately northwest-southeast. Such terrain can result in a funneling phenomenon when wind blows over the area, increasing the wind speed (Dong et al., 2014). The site is located near the southwest edge of the Badain Jaran desert, with the Taklimakan desert to the west. As shown in Fig. 1, this location is also affected by human activities focusing on agriculture and animal husbandry. The climate over there is dry and lacking in rain, along with strong evaporation under ample sunshine (Xuan et al., 2000).

It was mostly fair to cloudy during the sampling period, except for a severe sand-dust storm from 09:00 p.m. on the 23rd to 02:00 p.m. on the 25th April (shaded area in Fig. 2) and two floating dust episodes

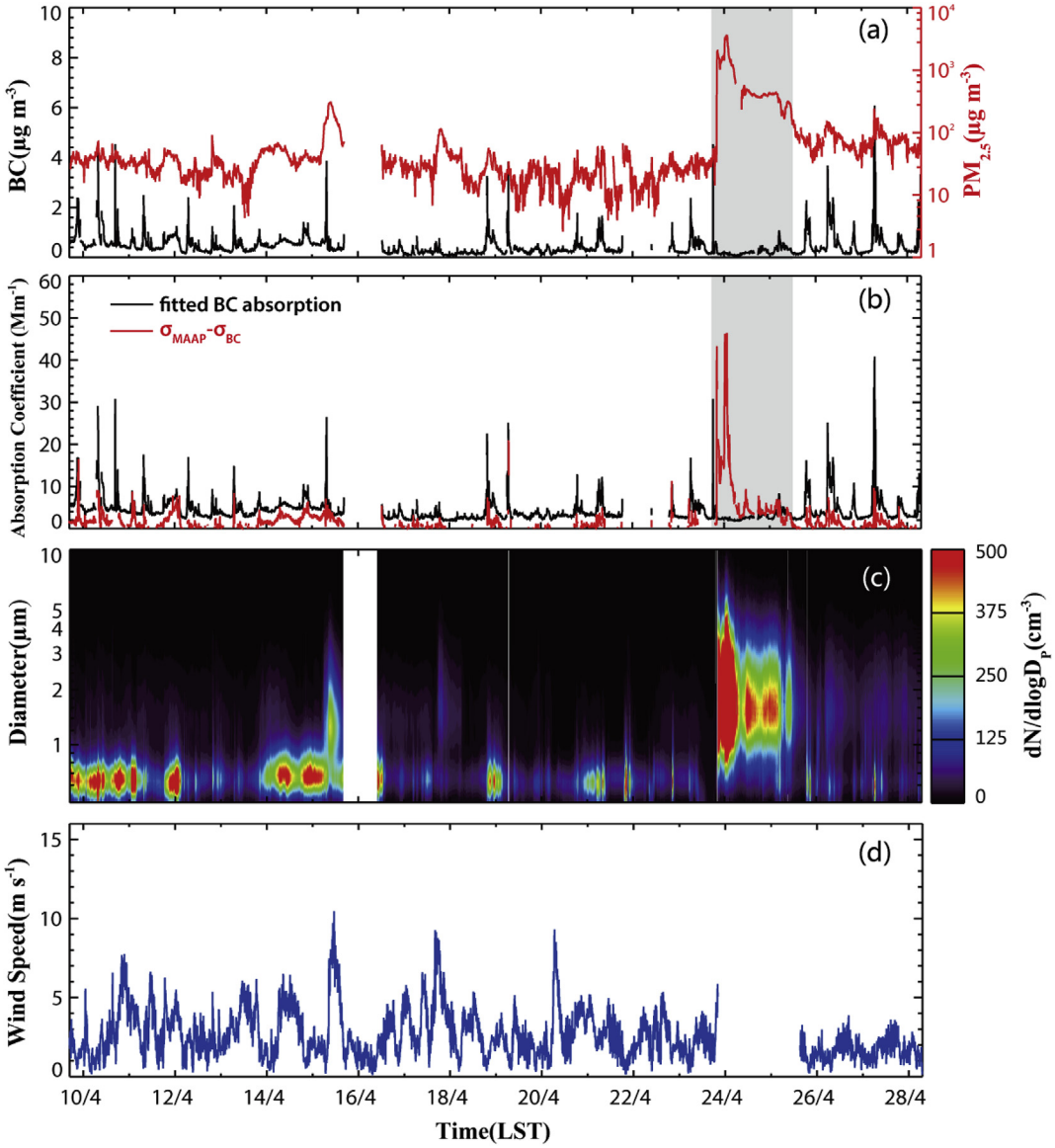

Fig. 2. The time series of aerosol characteristic parameters: a) mass concentrations of BC and $PM_{2.5}$; b) absorption coefficients (σ_{ap}) of the fitting BC and the discrepancy between MAAP σ_{ap} and the fitted BC σ_{ap}; c) aerosol size distribution ($dN/d\log Dp$, 0.5 μm < D_p < 10 μm); (d) wind speed during the entire survey from 9 to 28 April 2014. The shaded box represents a strong dust storm.

during 14–15 (from 06:30 a.m. on the 14th to 06:00 a.m. on the 15th) and 25–28 April, presenting differences in aerosols macroscopic distribution. Dust storm is defined as a kind of weather phenomenon accompanied by a sharp and distinct increase in wind speed and dust particles concentration, which reduce the horizontal visibility to less than 1 km (Zhang et al., 2005). When the dust storm or blowing sand process weaken, suspended dust particles in the lower troposphere cause a phenomenon generally defined as floating dust, with the horizontal visibility less than 10 km. Apart from the dust storm and floating dust episodes, the rest of days were defined as non-dust days (certain data influenced by fugitive dust was excluded). The westerly wind remained dominant nearly throughout the experiment with the mean wind speed of 2.61 m s^{-1}. In the perspective of diurnal variation, the strongest winds occurred from 10:00 to 12:00 a.m. (Local Standard Time). Then, the winds decreased gradually after 6:00 p.m. The average temperature was 11.97 °C and the minimum temperature was reached at approximately 07:00 a.m. while the maximum at approximately 02:00 p.m. The relative humidity showed a reverse diurnal variation pattern to the temperature, with a mean value of 35.63%.

2.2. BC mass measurement

All data were sampled in the SACOL from 5-min averages with a sampler inlet installed on the top of the laboratory, and placed 6.5 m above the ground (Wang et al., 2018b). After the unified collection by the inlet, aerosol samples were diverted into various instruments through the use of 1-μm and 2.5-μm cutoff impactors. The mass concentration of BC was obtained using a Single Particle Soot Photometer (SP2, Droplet Measurement Technology, Boulder, CO, USA) operated at a low flow rate of 0.12 L min^{-1}. Adjoined to the 1 μm impactor, the SP2 guides airborne particles with aerodynamic diameter less than 1 μm through a Nd:YAG laser cavity by a jet, and the laser beam (at 1064 nm) heats the particle causing it to incandesce (Stephens et al., 2003). By analyzing the laser-induced incandescence (LII) light and scattered light that four sensors detect, we can determine the optical size of every single particle, then take the BC mass converted from calibrated peak intensity of the incandescence signal. More details for the principles of SP2 can be found in Schwarz et al. (2006). By assuming the effective density of atmospheric BC as 1.8 g cm^{-3} (Bond and Bergstrom, 2006),

the size of the BC core, which is called the mass equivalent diameter, ranges from 120 to 650 nm in this campaign. Measurements of the BC based on SP2 approximately cover 90% of the BC size distribution in the ambient atmosphere via a lognormal fitting. To settle this systematic underestimation of BC mass, we estimate the total BC by extrapolating the size distribution on the basis of a single lognormal mode. On account of the uncertainties in the BC mass calibration, flow measurement and estimation of BC mass outside the scope of SP2 detection, there is an uncertainty of ~25 percent in the BC mass determination (Wang et al., 2014; Wu et al., 2016).

2.3. Aerosol absorption measurement

A multi-angle absorption photometer (MAAP, model-5012, Thermo Scientific, Waltham, MA, USA) was employed to quantify the aerosol absorption coefficients (σ_{ap}) of particles smaller than 2.5 μm in aerodynamic diameter at 637 nm. The MAAP has improved the filter-based measuring method of aerosol optical absorption and it considerably eliminates the light scattering impacts through off-axis detection at multiple angles (Petzold and Schönlinner, 2004). By employing an empirical conversion factor ($6.6\ m^2\ g^{-1}$), the equivalent mass concentration of BC (M_{BC}) is finally recorded by the MAAP according to the measured variation in the transmission through the filter. Nonetheless, the determined BC concentration is usually overestimated because other aerosol components (i.e., BrC and dust) may also contribute to the light absorption. Meanwhile, scattering material coatings also increase the absorption of BC, resulting in an additional overestimation in the determined M_{BC}. Slowik et al. (2007) demonstrated that the MAAP measurement of optically absorbing mass for uncoated soot particles was higher by ~50% than that measured by SP2, and a thicker anthracene coating may further increase the MAAP by ~20%. This discrepancy reached ~72% on non-dust days in our survey. The instantaneous aerosol absorption coefficient was employed in this study; thus, the following equation is used to convert the measured BC concentration back to aerosol absorption coefficient:

$$\sigma_{ap} = 6.6 M_{BC} \tag{1}$$

2.4. Auxiliary measurements

In addition, a tapered element oscillating microbalance (TEOM, model-1400a, R&P Corp., Albany, NY, USA) was used to measure the mass concentration of $PM_{2.5}$ simultaneously, at the flow rate of $16.7\ L\ min^{-1}$ controlled by a cyclone cutoff. A three-wavelength integrating nephelometer (model-3563, TSI Inc., Shoreview, MN, USA) with 2.5-μm cutoff was employed to obtain the aerosol scattering coefficients, for the purpose of calculating the refractive index of dust. Moreover, the aerosol number distribution (defined as $dN/dlogD_p$) was collected in real time by an aero-dynamical particle sizer (APS, model-3321, TSI Inc., Shoreview, MN, USA) that uses a sophisticated time-of-flight technique and can determine the size ranging from 0.5 to 20 μm via 51 channels. To obtain a better analysis of the data above from various aspects, a meteorological sensor (WXT-520, Vaisala Inc., Helsinki, Finland) was used to collect meteorological elements, such as ambient pressure, temperature, relative humidity, wind direction and wind speed, in real time. To ensure the accuracy of the data in this observation campaign, all datasets were adjusted to standard temperature and pressure conditions and subjected to quality control and calibration.

2.5. Data analysis methods

The mass absorption efficiency, defined as the absorption coefficient induced by unit mass of aerosol or certain aerosol component, is a key parameter for precisely demonstrating the radiative forcing of BC and other light absorbing materials (i.e., BrC and dust) and for a better understanding of their effects on climate. The bulk of MAE analyzed in this study is calculated as the slope of regressive and moving average model linear regression of absorption coefficient against the aerosol or certain aerosol component (e.g., BC or dust) mass concentration, which is expressed as:

$$MAE = \sigma_{ap}/C \tag{2}$$

where σ_{ap} is the absorption coefficient of aerosol or that induced by a certain aerosol component at 637 nm, and C is the corresponding mass concentration.

Different chemical compositions of aerosol particles in the real atmosphere result in a considerable variation in the imaginary part. In the paper, we inverted the dust refraction index ($m = n - ki$) by using Mie scattering theory, assuming spherical particles. Making use of the Ångström law, we converted the scattering coefficient (σ_{sp}) to 637 nm (Wang et al., 2018b).

Combining the scattering efficiency (Q_{sp}), the absorption efficiency (Q_{ap}) and the number distribution $n(logD_P)$ from APS, the computed values of scattering and absorption coefficients were acquired by MATLAB algorithms (Mätzler, 2002):

$$\sigma_{sp} = \int Q_{sp}(x,\ m)\quad n(logD_p)\quad \pi\left(\frac{D_p}{2}\right)^2\quad d\ logD_p \tag{3}$$

$$\sigma_{ap} = \int Q_{ap}(x,\ m)\quad n(logD_p)\quad \pi\left(\frac{D_p}{2}\right)^2\quad d\ logD_p \tag{4}$$

where D_p is the particle diameter and $x = \pi D_P/\lambda$ is the particle size parameter. To determine the most appropriate refractive index, we transformed the real part (n) within an appropriate range (1.30–2.00), while the imaginary component (k) varied from 0i to 0.1i (Woodward, 2001; Haywood, 2003).

Comparing the measured values of scattering coefficient (σ_{sp}^m) and absorption coefficient (σ_{ap}^m) with the calculated ones, respectively, relative differences between them can be defined as follow:

$$\varepsilon_{sp} = (\sigma_{sp} - \sigma_{sp}^m)/\sigma_{sp}^m \tag{5}$$

$$\varepsilon_{ap} = (\sigma_{ap} - \sigma_{ap}^m)/\sigma_{ap}^m \tag{6}$$

$$\varepsilon = \sqrt{(\varepsilon_{sp}^2 + \varepsilon_{ap}^2)/2} \tag{7}$$

Based on a series of postulated values for refractive index and the differences shown as Eq. (7), the refraction index that corresponded to the minimum value of relative deviations was regarded as the actual one of the measured airborne aerosols.

3. Results and discussion

3.1. Overview of BC concentration and aerosol absorption coefficient

The time-series of $PM_{2.5}$ and BC concentration are shown at 5-min intervals in Fig. 2a. The mean BC mass concentration (± standard deviation) for the entire campaign period was 443 ± 12 $ng\ m^{-3}$, accounting for ~0.4% of the $PM_{2.5}$. It was one order lower than those measured by the SP2 in the urban regions, such as Xi'an with a mean of 8.8 $\mu g\ m^{-3}$ (Wang et al., 2014) and Beijing with a mean of 5.5 $\mu g\ m^{-3}$ (Wu et al., 2016), while it was more than twice as high as the mean value of 160 ± 190 $ng\ m^{-3}$ observed in a remote area near the Tibetan Plateau reported by (Wang et al., 2015a). Our observation site received less pollution from local anthropogenic emissions than urban areas and a portion of the pollution came from regional transport. The aerosol absorption coefficient varied in a wide range between 1.09 and 52.81 Mm^{-1}, with an average value of 5.69 ± 0.01 Mm^{-1}.

As mentioned in section 2.1, different kinds of weather have their respective synoptic phenomena and visibility. To discuss aerosol optical properties under different weather conditions, we divided the data into three categories combined with ground observation records: non-dust

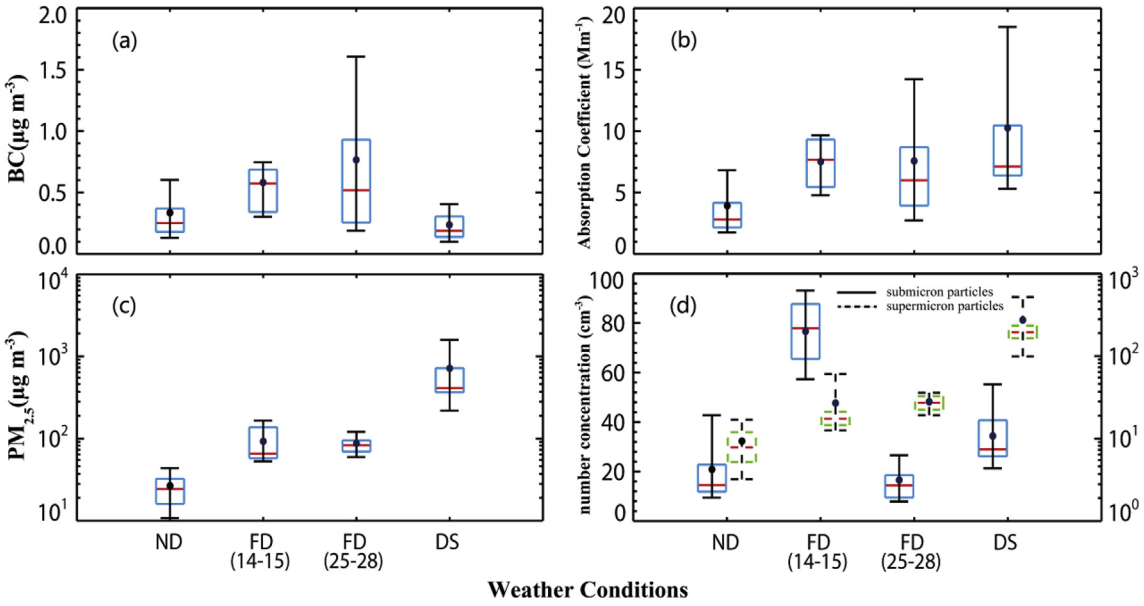

Fig. 3. The box and whisker plots show (a) BC concentration, (b) aerosol absorption coefficient, (c) $PM_{2.5}$ concentration and (d) number concentrations of submicron and supermicron particles during non-dust (ND) days, floating dust (FD) events and dust storm (DS), respectively. From the bottom up, the whiskers indicate the 10th and 90th percentiles, and the box lines indicate the 25th and 75th percentiles. The red lines and filled dots in the box represent the median and arithmetic mean values, respectively, for each weather condition. (For interpretation of the references to colour in this figure legend, the reader is referred to the Web version of this article.)

(ND) days, floating dust (FD) events and dust storm (DS). The mean BC and $PM_{2.5}$ mass concentration and absorption coefficient were 340 ng m^{-3}, 26 μg m^{-3} and 3.92 Mm^{-1} during ND days, suggesting the clean days unpolluted by dust. The submicron particles, of which the diameter was less than 1 μm, were predominant on ND days with the average number concentration more than twice that of the supermicron particles ranging in size larger than 1 μm (Fig. 3d). With the advent of dust plumes, $PM_{2.5}$ concentration significantly increased to 92 and 87 μg m^{-3} for two FD events on 14–15 and 25–28 April, respectively. Higher concentrations of BC were also observed during the FD episodes compared to those during the ND days (Fig. 3a), as can be expected due to wind-borne transmission of anthropogenic pollutants from southwest of the observatory, where the villages and roads were located in. The second FD episode immediately after the dust storm produced a greater BC concentration (765 ng m^{-3}) than the first one (581 ng m^{-3}), while its absorption coefficient (7.57 Mm^{-1}) was similar to that (7.51 Mm^{-1}) in the first FD episode (Fig. 3a and b). It is likely because the submicron particles remained predominant during the first FD episode; nevertheless, the supermicron particles constituted the majority of airborne aerosols during the second FD episode as the result of the dust storm influence. BC particles adhered on the surface of supermicron dust particles that absorbed less effectively than submicron ones.

The dust storm led to the consequence that the arithmetic mean of the mass concentration of $PM_{2.5}$ increased twenty times from that on ND days (Fig. 3c). In the peak period of the storm affected by dust plumes, the $PM_{2.5}$ mass concentration maintained at the level of heavy pollution above 500 μg m^{-3} and supermicron particles accounted for ~89% of the total. However, the mean concentration of BC declined to 237 ng m^{-3}, half of the clean level, during the dust storm. On the one hand, the dust-laden air masses that came from the northwestern desert regions contained very few BC particles. Meanwhile, the wind speed was higher during the sandstorm and had a diluting effect on the local BC concentration. On the other hand, many black carbon particles attached to the surface of large dust particles during the DS while the air inlet of SP2 was only 1 μm, which limited the scope of the observation. However, in comparison with the ND periods, the mean value of aerosol absorption coefficient increased by a factor of 2.6 during the storm (10.28 Mm^{-1}). Considering the reduction in BC concentration during the DS, the increase in the absorption coefficient was likely related to the contribution of other aerosol components, i.e., dust particles.

3.2. Mass absorption efficiency of BC particles

It was important to perform the correlation analysis of aerosol absorption coefficient and mass concentration because MAE was served as one of the primary optical properties of aerosol. Taking into account BC as the dominant light absorber among atmospheric aerosols, in general, aerosol absorption coefficient is remarkably correlated with BC mass concentration. The linear relationship appeared to be better when the dust events were excluded. To identify the relation of absorption with certain aerosol concentration, diurnal variations of BC and $PM_{2.5}$ mass concentration are shown in Fig. S1 separated into ND days and DS process, as well as the aerosol absorption coefficient. The variation in absorption coefficient is shown synchronously in a similar bimodal pattern with the BC concentration on ND days, indicating that BC was the dominant absorbing component. The dominant peak came out approximately between 07:00–08:00 a.m. during the commuting hours of traffic emission and residential combustion. As is demonstrated in Fig. S1b, there is an abrupt decrease in BC concentration during the DS and then it remains at a low level without obvious peak for the whole storm period. However, the variation trend of absorption coefficient is almost consistent with that of $PM_{2.5}$, increasing considerably in the DS. This result implies that the abundant dust particles had a great contribution to the aerosol absorption coefficient at the MAAP measuring wavelength of 637 nm (Kanaya et al., 2013).

As it is dominated by BC, the aerosol absorption coefficient shows a significant linear relation with the BC concentration during the ND period (square symbols in Fig. 4), with the square of correlation coefficients (R^2) of 0.94. This linear relationship is more robust at the morning peak (07:00–09:00 a.m. local time) with $R^2 = 0.97$ (red squares in Fig. 4), implying the absolute dominance of BC in the aerosol absorption coefficient. Accordingly, the bulked MAE of BC was derived to be 8.5 ± 1.1 m^2 g^{-1} at 637 nm (calculated as the slope of the linear regression of the absorption coefficient against the BC concentration). It is lower than the previous value measured by (Liu et al., 2010) in Switzerland (10.2 ± 3.2 m^2 g^{-1} at 630 nm) utilizing the same

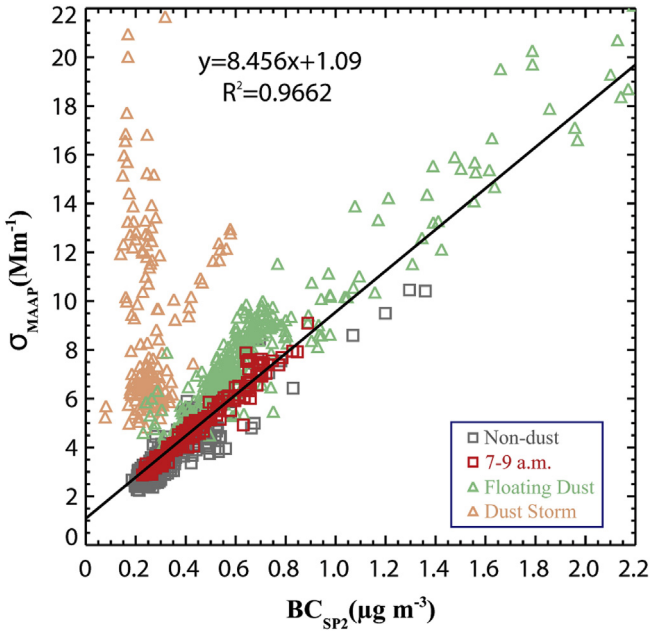

Fig. 4. The linear relationship between the absorption coefficient of MAAP and the BC mass concentration measured by SP2. The squares represent all the data on non-dust days and the data from 07:00 a.m. to 09:00 a.m. are marked in red. The triangles represent the data affected by dust weather (i.e., floating dust episodes and dust storm). (For interpretation of the references to colour in this figure legend, the reader is referred to the Web version of this article.)

approach. Employing the power-law relationship with the incident wavelength, the MAE reported in this study is estimated to be 9.8 $m^2 g^{-1}$ at 550 nm, much higher than that of the bare black carbon (7.5 ± 1.2 $m^2 g^{-1}$, Bond and Bergstrom, 2006). This may result from the different sources of aerosols and diverse mixing states of BC. Small particle sizes and thick coatings with scattering compounds on BC particles enhance the MAE of BC (Adler et al., 2010). The y-intercept of the linear regression presented in Fig. 4 might represent the measurement biases. The absorption coefficients in the $PM_{2.5}$ were measured, while the BC concentrations in the PM_1 were determined. Although the BC was mainly distributed in the submicron particles, the BC-containing particles in the size range of 1 μm < D_p < 2.5 μm also have a slight additional contribution to the absorption of $PM_{2.5}$.

Direct emissions from incomplete combustion of fossil fuel and biomass burning or secondary generation via atmospheric chemical reactions can also produce BrC (Andreae and Gelencser, 2006; Chakrabarty et al., 2010). Kirchstetter and Thatcher (2012) pointed that BrC has effective absorption in the near UV wavelength range, and because the overwhelming majority of aerosol absorption above ~700 nm is attributed to BC, we gave no consideration to the issue concerning BrC aerosols.

3.3. Contribution of dust particles

As shown in Fig. 4, in the FD and DS events, the aerosol absorption coefficient significantly deviated from its linear relation with the BC concentration during ND periods, demonstrating the dust particles contributed substantially to light absorption. To assess the contribution of dust particles to absorption, the time-resolved absorption coefficients induced by BC were first estimated from the derived MAE of BC (8.5 $m^2 g^{-1}$ at 637 nm) and the measured BC concentrations by SP2. Then, by subtracting the BC absorption coefficients from the measured ones by MAAP, the absorption coefficients induced by dust particles were obtained (Fig. 2b). On the average, the dust absorption brought approximately 26.7% of the total throughout the observation and this percentage was 16.5% on ND day. An increment value of 14.9% and

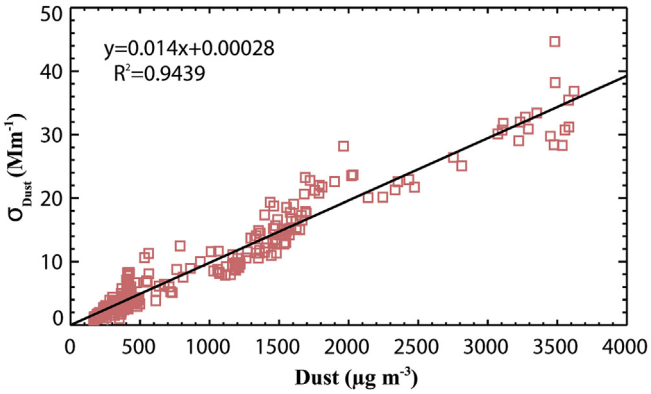

Fig. 5. The linear relationship between absorption coefficient of dust and its mass concentration during the dust storm.

14.2% for dust aerosols occurred in two FD episodes, while the mean absorption induced by dust increased to 7.36 Mm^{-1} during the DS, which made up 71.6% of atmospheric aerosol absorption. This result indicated that dust exerted considerable positive influence on the light absorption. Previous work has shown that the absorption of dust particles has a greater proportion of the gross absorption during dust weather (Fialho et al., 2005). It can be seen that the difference abruptly increases to an extremely high value when the dust storm occurs because the atmospheric aerosol component is dominated by dust to a large extent, playing a vital role in the absorption of the solar spectrum.

3.4. Mass absorption efficiency and refractive index of dust particles

Now that only 0.03% of the $PM_{2.5}$ mass concentration was attributed to BC in the DS process, $PM_{2.5}$ concentration can be a substitute for dust mass concentration. To highlight the absorptive characteristics of dust aerosols, we utilized the aforementioned absorption coefficient of dust aerosols during the DS, determining the value of its MAE associated with the corresponding mass concentration. According to the linear least squares method, the MAE of dust aerosol was estimated at 0.014 ± 0.00028 $m^2 g^{-1}$ at 637 nm (shown in Fig. 5, R^2 = 0.94). It is commonly considered that the absorption efficiency of dust decreases with the increase in wavelength, with the highest absorption ability of dust at ~440 nm (Todd et al., 2007). The MAE of dust particles tend to range from 0.02 to 0.1 $m^2 g^{-1}$ at 550 nm (Antony and Robert, 1985). Additionally, a typical calculation was once made for the dust absorption from 470 nm to 660 nm, and the value at 660 nm was reckoned at ~0.013 $m^2 g^{-1}$ (Yang et al., 2009). Even though the light absorption efficiency for dust was much lower than that for black carbon (~8.5 $m^2 g^{-1}$ at 637 nm), its contribution to total absorption can be on the same order of magnitude as that of the BC during dust events owing to the huge amounts of suspended dust particles in the air. As previously stated, in three events aerosol absorption coefficients were all increased in different degrees.

Allowing for the fact that dust aerosols formed the principal part of the sandstorm, it was generally assumed that number distribution, measured absorption and scattering coefficients were all attributed to dust during that period. On the basis of theoretical calculations applying the model of Mie theory, we processed the relevant datasets during the DS, adjusting the real and imaginary parts of the refraction index to make the calculated values proximate to the true values, both in the aspects of scattering coefficient and absorption coefficient. When there are a large number of coarse-mode particles in the atmosphere (e.g., dust particles), the dependence of the absorption and scattering characteristics on the refractive index is complex (Balkanski et al., 2007). As such, we attained the actual imaginary part of the refraction index (at 637 nm) for natural mineral dust aerosols during the storm (sources from Taklimakan Desert and Badain Jaran Desert) with the

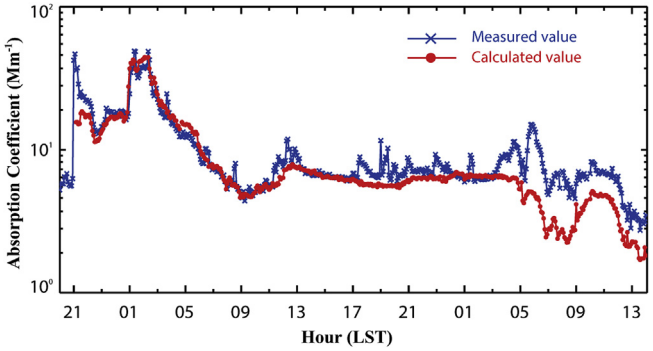

Fig. 6. The measured values of aerosol absorption coefficient and the corresponding calculated values based on Mie theory during the dust storm (23–25 April).

value of 0.0007, and its real part was derived as 1.50. For spherical and non-spherical particles, the difference between their absorption cross sections is only ~2% (Mishchenko et al., 1997), suggesting that these refractive indices apply equally to irregular dust particles. As is delineated in Fig. 6, some differences between the measured and computed values in the later part of the dust storm can be explained by a presence of other anthropogenic aerosols such as BC, since the weather gradually turned into the floating dust after the passage of storm. However, when the computed values were based on the pure dust particles, the actual mixture led to more absorption than expected. To some extent, the magnitude of the dust refractive index, particularly of its imaginary part, differs according to particle mineralogical composition from varying emissions sources (Di Biagio et al., 2014). This can interpret the variation range of imaginary component from 0.0003 to 0.0052 at 550 nm (Woodward, 2001). Clarke (2004) reported a value of 0.0006 at ~550 nm for the imaginary part of the dust refraction index in Asia. Furthermore, the imaginary part and real part at 675 nm for pure dust were inferred to be 0.0016 and 1.53 on average over East and Central Asian areas, respectively (Bi et al., 2016). By the comparison with our computational results, it indicates that the imaginary part involve a greater uncertainty than the real part (Dubovik et al., 2002). Diverse inversion methods may bring about inconsistencies in the final results as well. However, the value of imaginary part was lower than the 0.008 recommended by (World Meteorological Organization, 1986), probably due to the various dust sources and chemical compositions of dust aerosols. The investigation over the Asia-north Pacific region found that the imaginary part of the refractive index of East Asian dust was also smaller than the OPAC-model (Wang et al., 2004), implying that dust aerosols emitted from Chinese deserts absorb less solar radiation than the most dust optical models published so far. Above the 670 nm wavelength, the imaginary part of the mineral dust almost remains the invariant. Even though our value for the imaginary part was small, large particle size and great quantities for dust particles from the desert areas improved the dust MAE in Zhangye. Mineral dust is a kind of weakly absorbing aerosol, of which the MAE is 2–3 orders of magnitude lower than that of BC; however, it makes significant contribution to total aerosol absorption in solar spectrum and undoubtedly cannot be overlooked. Therefore, the mass absorption efficiency and the imaginary part of the refractive index for dust aerosol calculated in this study can provide the effective theoretical foundation for future model application and other work. It will help reduce errors arising in the accurate assessments of aerosol radiative forcing over arid and semiarid regions.

4. Conclusions

In this study, we focused on the absorption efficiency of dust and BC aerosols, and classified the atmospheric conditions into ND days, FD episodes and DS to differentiate varieties of aerosols absorption capacities. Throughout the whole investigation period, we acquired mean values of $PM_{2.5}$ and BC mass concentration of 103 ± 4 μg m^{-3} and 443 ± 12 ng m^{-3}, respectively. Influenced by less discharge of air pollutants, the measured BC concentration was markedly lower than those in urban regions. The ND days and the first FD event were dominated by submicron particles, while particles in the supermicron mode were the predominant type in the DS and the second FD period (affected by the sandstorm). High concentrations of BC appeared in the FD episodes instead of ND days owing to the transport of anthropogenic pollutants from surrounding villages and roads. In contrast, during the dust storm, there was a decline in the BC mass concentration, with the average value half that on the ND days. The reduced concentration was caused by dilution effect of strong winds, along with few BC particles blown from the desert regions. In addition, the detection range of SP2 was relatively limited for BC with large sizes. The value of σ_{ap} varied over a wide range (1.09–52.81 Mm^{-1}) during the field survey, with an average of 5.69 ± 0.01 Mm^{-1}. It is worth noting that σ_{ap} exhibited a significant increase during dust events, especially during the sandstorm, showing that dust generated substantial absorption which is equally important as the absorption by BC.

Combined with diurnal variations for BC and $PM_{2.5}$ concentration and aerosol σ_{ap}, a strong linear relation was observed between BC mass concentration and σ_{ap} of 07:00–09:00 a.m. on ND days, from which the MAE of BC was deduced as 8.5 ± 1.1 m^2 g^{-1}. The coatings on BC particles can partly enhance their absorption. For the ND days, FD events and DS process, the proportion of dust absorption in the overall amount presented an increasing trend, 16.5%, 31.1% and 71.6%, respectively. The large increase in the sandstorm verified the great contribution of dust to absorption in the red and near-infrared regions of the light spectrum. With $PM_{2.5}$ concentration serving as dust concentration during the DS process, the MAE of dust aerosol at 637 nm can be reckoned as 0.014 ± 0.00028 m^2 g^{-1}. In reference to the spherical Mie theory, we calculated the real part (1.50) and imaginary part (0.0007) of the refractive index for natural dust. Although the absorption by dust particles is inherently less efficient compared with BC, dust aerosol is considered crucial to the total absorption of solar radiation, particularly during dust events.

Data availability

All datasets used to produce this work can be obtained by contacting Xin Wang (wxin@lzu.edu.cn).

Acknowledgements

This work was supported by the National Natural Science Foundation of China (No. 41575150, 41775155, 41522505 and 41775144), and the Fundamental Research Funds for the Central Universities (No. lzujbky-2018-k05).

Appendix A. Supplementary data

Supplementary data related to this article can be found at http://dx.doi.org/10.1016/j.atmosenv.2018.07.002.

References

Adler, G., Riziq, A.A., Erlick, C., Rudich, Y., 2010. Effect of intrinsic organic carbon on the optical properties of fresh diesel soot. Proc. Natl. Acad. Sci. Unit. States Am. 107, 6699–6704.
Alexander, D.T., Crozier, P.A., Anderson, J.R., 2008. Brown carbon spheres in East Asian outflow and their optical properties. Science 321, 833–836.
Andreae, M.O., 1996. Raising dust in the greenhouse. Nature 380, 340–389.
Andreae, M.O., Gelencser, A., 2006. Black carbon or brown carbon? The nature of light-absorbing carbonaceous aerosols. Atmos. Chem. Phys. 6, 3131–3148.
Antony, D.C., Robert, J.C., 1985. Radiative properties of the background aerosol-absorption component of extinction. Science 229, 263–265.

Balkanski, Y., Schulz, M., Claquin, T., Guibert, S., 2007. Reevaluation of Mineral aerosol radiative forcings suggests a better agreement with satellite and AERONET data. Atmos. Chem. Phys. 7, 81–95.
Bergstrom, R.W., Pilewskie, P., Russell, P.B., Redemann, J., Bond, T.C., Quinn, P.K., Sierau, B., 2007. Spectral absorption properties of atmospheric aerosols. Atmos. Chem. Phys. 7, 5937–5943.
Bi, J., Huang, J., Holben, B., Zhang, G., 2016. Comparison of key absorption and optical properties between pure and transported anthropogenic dust over East and Central Asia. Atmos. Chem. Phys. 16, 15501–15516.
Bond, T.C., Bergstrom, R.W., 2006. Light absorption by carbonaceous particles: an investigative review. Aerosol Sci. Technol. 40, 27–67.
Boucher, O., Randall, D., Artaxo, P., Bretherton, C., Feingold, G., Forster, P., Kerminen, V.-M., Kondo, Y., Liao, H., Lohmann, U., Rasch, P., Satheesh, S.K., Sherwood, S., Stevens, B., Zhang, X.Y., 2013. Clouds and aerosols. In: Climate Change 2013: the Physical Science Basis. Contribution of Working Group I to the Fifth Assessment Report of the Intergovernmental Panel on Climate Change. Cambridge University Press, Cambridge, United Kingdom and New York.
Cao, X., Liang, J., Tian, P., Zhang, L., Quan, X., Liu, W., 2014. The mass concentration and optical properties of black carbon aerosols over a semi–arid region in the northwest of China. Atmos. Pollut. Res. 5, 601–609.
Chakrabarty, R.K., Moosmüller, H., Chen, L.W.A., Lewis, K., Arnott, W.P., Mazzoleni, C., Dubey, M.K., Wold, C.E., Hao, W.M., Kreidenweis, S.M., 2010. Brown carbon in tar balls from smoldering biomass combustion. Atmos. Chem. Phys. 10, 6363–6370.
Choobari, O.A., Zawar-Reza, P., Sturman, A., 2014. The global distribution of mineral dust and its impacts on the climate system: a review. Atmos. Res. 138, 152–165.
Clarke, A.D., 2004. Size distributions and mixtures of dust and black carbon aerosol in Asian outflow: physiochemistry and optical properties. J. Aerosol Sci. 109 D15S09.
Di Biagio, C., Formenti, P., Styler, S.A., Pangui, E., Doussin, J.F., 2014. Laboratory chamber measurements of the longwave extinction spectra and complex refractive indices of African and Asian mineral dusts. Geophys. Res. Lett. 41, 6289–6297.
Dong, A., Hu, W., Zhang, Y., 2014. Study of the relationship between gale and the peculiar terrain in the Hexi Corridor. J. Glaciol. Geocryol. 36, 347–351.
Dubovik, O., Holben, B., Eck, T.F., Smirnov, A., Kaufman, Y.J., King, M.D., Tanre´, D., Slutsker, I., 2002. Variability of absorption and optical properties of key aerosol types observed in worldwide locations. J. Aerosol Sci. 59, 590–607.
Falkovich, A.H., 2004. Adsorption of organic compounds pertinent to urban environments onto mineral dust particles. J. Geophys. Res. 109 D02208.
Fialho, P., Hansen, A.D.A., Honrath, R.E., 2005. Absorption coefficients by aerosols in remote areas: a new approach to decouple dust and black carbon absorption coefficients using seven-wavelength Aethalometer data. J. Aerosol Sci. 36, 267–282.
Haywood, J., 2003. Radiative properties and direct radiative effect of Saharan dust measured by the C-130 aircraft during SHADE: 1. Solar spectrum. J. Geophys. Res. 108 (D18), 8577.
Huang, J., Minnis, P., Lin, B., Wang, T., Yi, Y., Hu, Y., Sun-Mack, S., Ayers, K., 2006. Possible influences of Asian dust aerosols on cloud properties and radiative forcing observed from MODIS and CERES. Geophys. Res. Lett. 33, 272–288.
Huang, J., Wang, T., Wang, W., Li, Z., Yan, H., 2014. Climate effects of dust aerosols over East Asian arid and semiarid regions. J. Geophys. Res. 119, 398–416.
Husar, R.B., Tratt, D.M., Schichtel, B.A., Falke, S.R., Li, F., Jaffe, D., Gassó, S., Gill, T., Laulainen, N.S., Lu, F., Reheis, M.C., Chun, Y., Westphal, D., Holben, B.N., Gueymard, C., McKendry, I., Kuring, N., Feldman, G.C., McClain, C., Frouin, R.J., Merrill, J., DuBois, D., Vignola, F., Murayama, T., Nickovic, S., Wilson, W.E., Sassen, K., Sugimoto, N., Malm, W.C., 2001. Asian dust events of April 1998. J. Geophys. Res. 106, 317–330.
Jeong, G.Y., 2008. Bulk and single-particle mineralogy of Asian dust and a comparison with its source soils. J. Geophys. Res. 113 D02208.
Kanaya, Y., Taketani, F., Komazaki, Y., Liu, X., Kondo, Y., Sahu, L.K., Irie, H., Takashima, H., 2013. Comparison of black carbon mass concentrations observed by multi-angle absorption photometer (MAAP) and continuous soot-monitoring system (COSMOS) on Fukue Island and in Tokyo, Japan. Aerosol Sci. Technol. 47, 1–10.
Kirchstetter, T.W., Novakov, T., Hobbs, P.V., 2004. Evidence that the spectral dependence of light absorption by aerosols is affected by organic carbon. J. Geophys. Res. 109 D21208.
Kirchstetter, T.W., Thatcher, T.L., 2012. Contribution of organic carbon to wood smoke particulate matter absorption of solar radiation. Atmos. Chem. Phys. 12, 6067–6072.
Lan, Z.J., Huang, X.F., Yu, K.Y., Sun, T.L., Zeng, L.W., Hu, M., 2013. Light absorption of black carbon aerosol and its enhancement by mixing state in an urban atmosphere in South China. Atmos. Environ. 69, 118–123.
Laurent, B., Marticorena, B., Bergametti, G., Léon, J.F., Mahowald, N.M., 2008. Modeling mineral dust emissions from the Sahara desert using new surface properties and soil database. J. Geophys. Res. 113 D14218.
Liu, D., Flynn, M., Gysel, M., Targino, A., Crawford, I., Bower, K., Choularton, T., Jurányi, Z., Steinbacher, M., Hüglin, C., Curtius, J., Kampus, M., Petzold, A., Weingartner, E., Baltensperger, U., Coe, H., 2010. Single particle characterization of black carbon aerosols at a tropospheric alpine site in Switzerland. Atmos. Chem. Phys. 10, 7389–7407.
Liu, Y., Huang, J., Shi, G., Takamura, T., Khatri, P., Bi, J., Shi, J., Wang, T., Wang, X., Zhang, B., 2011. Aerosol optical properties and radiative effect determined from sky-radiometer over Loess Plateau of Northwest China. Atmos. Chem. Phys. 11, 11455–11463.
Lukács, H., Gelencsér, A., Hammer, S., Puxbaum, H., Pio, C., Legrand, M., Kasper-Giebl, A., Handler, M., Limbeck, A., Simpson, D., Preunkert, S., 2007. Seasonal trends and possible sources of brown carbon based on 2-year aerosol measurements at six sites in Europe. J. Geophys. Res. 112 D23S18.
Mätzler, C., 2002. MATLAB Functions for Mie Scattering and Absorption. Institut für Angewandte Physik, Bern Schweiz.
Mishchenko, M.I., Travis, L.D., Kahn, R.A., West, R.A., 1997. Modeling phase functions for dustlike tropospheric aerosols using a shape mixture of randomly oriented polydisperse spheroids. J. Geophys. Res. 102, 16831–16847.
Niu, S.J., Zhang, Q.Y., 2010. Scattering and absorption coefficients of aerosols in a semi-arid area in China: diurnal cycle, seasonal variability and dust events. Asia-Pac. J. Atmos. Sci. 46, 65–71.
Novakov, T., Ramanathan, V., Hansen, J.E., Kirchstetter, T.W., Sato, M., Sinton, J.E., Sathaye, J.A., 2003. Large historical changes of fossil-fuel black carbon aerosols. Geophys. Res. Lett. 30, 1324.
Oshima, N., Koike, M., Zhang, Y., Kondo, Y., Moteki, N., Takegawa, N., Miyazaki, Y., 2009. Aging of black carbon in outflow from anthropogenic sources using a mixing state resolved model: model development and evaluation. J. Geophys. Res. 114 D06210.
Petzold, A., Schönlinner, M., 2004. Multi-angle absorption photometry—a new method for the measurement of aerosol light absorption and atmospheric black carbon. J. Aerosol Sci. 35, 421–441.
Pu, W., Wang, X., Zhang, X., Ren, Y., Shi, J.S., Bi, J.R., Zhang, B.D., 2015. Size distribution and optical properties of particulate matter (PM_{10}) and black carbon (BC) during dust storms and local air pollution events across a loess plateau site. Aerosol Air Qual. Res. 15, 2212–2224.
Ram, K., Sarin, M.M., 2009. Absorption coefficient and site-specific mass absorption efficiency of elemental carbon in aerosols over urban, rural, and high-altitude sites in India. Environ. Sci. Technol. 43, 8233–8239.
Ramanathan, V., Carmichael, G., 2008. Global and regional climate changes due to black carbon. Nat. Geosci. 1, 221–227.
Schwarz, J.P., Gao, R.S., Fahey, D.W., Thomson, D.S., Watts, L.A., Wilson, J.C., Reeves, J.M., Darbeheshti, M., Baumgardner, D.G., Kok, G.L., Chung, S.H., Schulz, M., Hendricks, J., Lauer, A., Kärcher, B., Slowik, J.G., Rosenlof, K.H., Thompson, T.L., Langford, A.O., Loewenstein, M., Aikin, K.C., 2006. Single-particle measurements of midlatitude black carbon and light-scattering aerosols from the boundary layer to the lower stratosphere. J. Geophys. Res. 111 D16207.
Slowik, J.G., Cross, E.S., Han, J.H., Davidovits, P., Onasch, T.B., Jayne, J.T., Williams, L.R., Canagaratna, M.R., Worsnop, D.R., Chakrabarty, R.K., Moosmüller, H., Arnott, W.P., Schwarz, J.P., Gao, R.-S., Fahey, D.W., Kok, G.L., Petzold, A., 2007. An intercomparison of instruments measuring black carbon content of soot particles. Aerosol Sci. Technol. 41, 295–314.
Sokolik, I.N., Toon, O.B., 1999. Incorporation of mineralogical composition into models of the radiative properties of mineral aerosol from UV to IR wavelengths. J. Geophys. Res. 104, 9423–9444.
Stephens, M., Turner, N., Sandberg, J., 2003. Particle identification by laser-induced incandescence in a solid-state laser cavity. Appl. Optic. 42, 3726–3736.
Su, J., Huang, J., Fu, Q., Minnis, P., Ge, J., Bi, J., 2008. Estimation of Asian dust aerosol effect on cloud radiation forcing using Fu-Liou radiative model and CERES measurements. Atmos. Chem. Phys. 8, 2763–2771.
Sullivan, R.C., Guazzotti, S.A., Sodeman, D.A., Prather, K.A., 2007. Direct observations of the atmospheric processing of Asian mineral dust. Atmos. Chem. Phys. 7, 1213–1236.
Todd, M.C., Washington, R., Martins, J.V., Dubovik, O., Lizcano, G., M'Bainayel, S., Engelstaedter, S., 2007. Mineral dust emission from the Bodélé depression, northern Chad, during BoDEx 2005. J. Geophys. Res. 112 D06207.
Uno, I., Eguchi, K., Yumimoto, K., Takemura, T., Shimizu, A., Uematsu, M., Liu, Z., Wang, Z., Hara, Y., Sugimoto, N., 2009. Asian dust transported one full circuit around the globe. Nat. Geosci. 2, 557–560.
Wang, H., Shi, G., Aoki, T., Wang, B., Zhao, T., 2004. Radiative forcing due to dust aerosol over east Asia-north Pacific region during spring, 2001. Chin. Sci. Bull. 49, 2212–2219.
Wang, Q., Huang, R.J., Cao, J., Han, Y., Wang, G., Li, G., Wang, Y., Dai, W., Zhang, R., Zhou, Y., 2014. Mixing state of black carbon aerosol in a heavily polluted urban area of China: implications for light absorption enhancement. Aerosol Sci. Technol. 48, 689–697.
Wang, Q.Y., Huang, R.J., Cao, J.J., Tie, X.X., Ni, H.Y., Zhou, Y.Q., Han, Y.M., Hu, T.F., Zhu, C.S., Feng, T., Li, N., Li, J.D., 2015a. Black carbon aerosol in winter northeastern Qinghai–Tibetan Plateau, China: the source, mixing state and optical property. Atmos. Chem. Phys. 15, 13059–13069.
Wang, X., Huang, J., Ji, M., Higuchi, K., 2008. Variability of East Asia dust events and their long-term trend. Atmos. Environ. 42, 3156–3165.
Wang, X., Pu, W., Shi, J., Bi, J., Zhou, T., Zhang, X., Ren, Y., 2015b. A comparison of the physical and optical properties of anthropogenic air pollutants and mineral dust over Northwest China. J. Meteorol. Res. 29, 180–200.
Wang, X., Liu, J., Che, H., Ji, F., Liu, J., 2018a. Spatial and temporal evolution of natural and anthropogenic dust events over northern China. Sci. Rep. 8, 2141.
Wang, X., Wen, H., Shi, J., Bi, J., Huang, Z., Zhang, B., Zhou, T., Fu, K., Chen, Q., Xin, J., 2018b. Optical and microphysical properties of natural mineral dust and anthropogenic soil dust near dust source regions over northwestern China. Atmos. Chem. Phys. 18, 2119–2138.
Woodward, S., 2001. Modeling the atmospheric life cycleand radiative impact of mineral dust in the Hadley Centre climate model. J. Geophys. Res. 106, 18155–18166.
World Meteorological Organization, 1986. A Preliminary Cloudless Standard Atmosphere for Radiation Computation. World Climate Program, Geneva WCP-112.
Wu, Y., Zhang, R., Tian, P., Tao, J., Hsu, S.C., Yan, P., Wang, Q., Cao, J., Zhang, X., Xia, X., 2016. Effect of ambient humidity on the light absorption amplification of black carbon in Beijing during January 2013. Atmos. Environ. 124, 217–223.
Xuan, J., Liu, G., Du, K., 2000. Dust emission inventory in northern China. Atmos. Environ. 34, 4565–4570.
Yang, M., Howell, S.G., Zhuang, J., Huebert, B.J., 2009. Attribution of aerosol light absorption to black carbon,brown carbon and dust in China. Atmos. Chem. Phys. 9, 2035–2050.
Zhang, R., Richard, A., Junling, A., Sadayo, Y., Jianhua, S., 2005. Ground observations of a strong dust storm in Beijing in March 2002. J. Geophys. Res. 110 D18S06.
Zhang, X.Y., Gong, S.L., Shen, Z.X., Mei, F.M., Xi, X.X., Liu, L.C., Zhou, Z.J., Wang, D., Wang, Y.Q., Cheng, Y., 2003. Characterization of soil dust aerosol in China and its transport and distribution during 2001 ACE-Asia: 1. Network observations. J. Geophys. Res. 108 D94261.